


Homogenous Microporous Thin Films Assembled Using Discrete Metal–Organic Polyhedra

Soyeon Ko, Unjin Ryu, Ho Yeon Yoo, Jeeyoung Shin, Kyung Min Choi*, Dong Gyu Park*, and Won Ho Choi* 

Homogeneous films with tailored microporous structures are crucial for several applications; however, fabricating such films presents significant challenges. This is primarily because most microporous materials have crystal sizes in the nano- and micrometer ranges, which inevitably generates intergranular spaces in the films, thereby complicating the fabrication of these thin films. In this study, functionalized metal–organic polyhedra (MOPs) are used as discrete microporous units and assembled into homogenous microporous films. The generation of intergranular spaces is avoided while controlling packing parameters and film thicknesses. Initially, the MOP units, influenced by van der Waals forces between carbon chains of functionalized adipic acids, display an affinity to form spindle-shaped blocks and islands. As the MOP concentration increases, these structures self-assembled into a hexagonally packed structure with an in-plane orientation and a maximum stacking of two layers of MOPs. By contrast, un-functionalized MOPs form a disordered film structure owing to random agglomeration. Evidently, functionalized adipic acid influences the orientation of the MOP network films with uniformly distributed micropores, effectively preventing the formation of intergranular spaces. Additionally, formaldehyde adsorption and desorption experiments revealed that the MOP network films possess superior adsorption and desorption capacities. The proposed approach signifies a breakthrough in the fabrication of homogenous microporous films.

1. Introduction

Homogenous films with tailored micropores have garnered considerable interest due to the predictable and optimized performances of these films in a variety of fields, including gas storage and catalysis.^[1–3] The superior performances of these films can be attributed to the uniform distribution of micropores throughout the films and the consistent interactions between the micropores and target molecules.^[4] Metal–organic frameworks (MOFs) are an attractive material for preparing homogenous microporous films, as MOFs possess designable pore structures and permanent micropores.^[5–9] To fabricate MOF-based films, various methods, including direct growth,^[10–13] coating processes,^[14–17] printing,^[18,19] and the use of composites,^[20,21] have been successfully explored. However, fabricating homogenous MOF film remains a considerable challenge due to the typical micrometer-scale crystal sizes of MOFs. This micrometer-sized material exhibits less efficient close-packing behavior than nanomaterials, leading to undesired heterogeneities owing to the presence of interparticle spaces,

grain boundaries, and cracks. More specifically, although MOFs inherently possess uniform micropores, structural intergranular spaces are inevitably formed when fabricating homogenous films. A promising solution involves constraining the microporous material to a discrete micropore system. By assembling the discrete micropore system into a uniform layered film, a homogenous microporous film devoid of the inherent limitations of typical MOF films can be realized.

Metal–organic polyhedra, commonly termed nano-cages, epitomize the concept of a discrete micropore system. MOPs typically possess the same pore system as that of MOFs made of organic linkers and metal nodes, and additional crystal growth is restricted by preventing the formation of interconnections.^[22,23] This distinctive feature retains the discrete micropore system and enables the high-level pore design of the films. Furthermore, the discrete MOP nanocages exhibit excellent processibility owing to their high solubility, which allows for the precise control of the uniform dispersion and concentration of MOPs in a solvent to be precisely controlled.^[24] These properties combined with a well-defined discrete pore structure and enhanced processibility render MOPs a promising candidate for fabricating homogenous microporous films. Although MOPs can be used for fabricating large super-frameworks,^[25,26] current methods have failed to assemble

S. Ko, Prof. K. M. Choi
Department of Chemical and Biological Engineering, Sookmyung Women's University, Cheongpa-ro 47-gil 100, Seoul 04310, Korea
E-mail: kmchoi@sookmyung.ac.kr


Dr. U. Ryu
Industry Collaboration Center, Sookmyung Women's University, Cheongpa-ro 47-gil 100, Seoul 04310, Korea

Dr. H. Y. Yoo
Department of Applied Chemistry, Andong National University, Gyeongdong-ro 1533-2, Andong-si 36729, Korea

Prof. J. Shin
Department of Mechanical Systems Engineering, Sookmyung Women's University, Cheongpa-ro 47-gil 100, Seoul 04310, Korea

Dr. D. G. Park
Institute of Advanced Materials and Systems, Sookmyung Women's University, Seoul 04310, Korea

E-mail: donggyu.park@sookmyung.ac.kr
Prof. W. H. Choi
Department of Petrochemical Materials, Chonnam National University, 19 Samdong 3-gil, Yeosu-si 59631, Korea

E-mail: wonhochoi@jnu.ac.kr
 The ORCID identification number(s) for the author(s) of this article can be found under <https://doi.org/10.1002/eem2.12805>.

DOI: 10.1002/eem2.12805

discrete MOPs into homogenous films. In this study, we added carbon chains to promote interactions between MOPs such that these MOPs can be assembled into a uniformly layered microporous film. Unlike the method that uses unfunctionalized MOPs, our strategy using functionalized MOPs with carbon chains uniformly distributes the discrete micropores, with specific orientations that can be controlled via enhanced close packing, throughout the films. A homogenous microporous MOP film was deposited on the surface of a quartz crystal microbalance (QCM), and the porosity of this film was determined. The frequency variations of the QCM indicated that the homogenous microporous MOP film absorbed 11- and twofold higher amounts of formaldehyde than the uncoated QCM and a non-homogenous MOP film, respectively, at ambient temperature.

2. Results and Discussion

Pristine Zr-based MOPs were synthesized as discrete nano-cages for fabricating homogenous microporous films. First, a Zr cluster ($[\text{Cp}_3\text{Zr}_3\text{O}(\text{OH})_3(\text{COO})_3]^+$) (here, Cp denotes cyclopentadienyl) was prepared by the hydrolyzing bis(Cp)ZrCl₂.^[25,27] The resulting Zr cluster ($[\text{Cp}_3\text{Zr}_3\text{O}(\text{OH})_3(\text{COO})_3]^+$) had six coordination points, three of which were capped by Cp molecules, leaving only three coordination points for connections with linkers.^[28] Subsequently, 2-aminoterephthalic acid (BDC-NH₂) ligands were added to the Zr-cluster solution to coordinate with the tritopic Zr clusters to form tetrahedral Zr-based MOPs (Figure 1a).

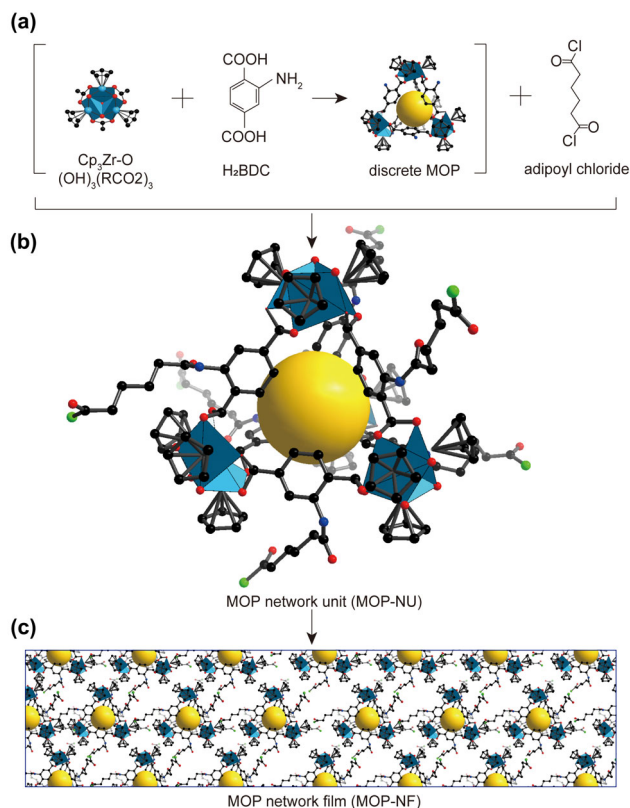


Figure 1. Schematic illustrations of the MOP-NUs and MOP-NFs.

The X-ray diffraction (XRD) patterns of the Zr-based MOPs display narrow peaks consistent with the simulated XRD patterns of MOP crystals (Figure 2a). Furthermore, the MOP crystals exhibit cubic morphologies, suggesting a periodic arrangement of the discrete MOPs, as shown in the field emission scanning electron microscope (FESEM) (Figure 2b) and optical microscope images (Figure S1, Supporting Information).^[25] The MOP crystals were highly crystalline and possessed a cubic morphology owing to the periodical arrangement of discrete MOPs, thereby evidencing the formation of the intended discrete MOP nanocages. The MOP crystals immersed in methanol (MeOH) were easily separated into discrete MOPs because the hydrogen bonds between the discrete MOPs were replaced by the strong interactions between the MOPs and MeOH.^[25] The XRD patterns that did not possess the aforementioned narrow peaks (Figure S2, Supporting Information) and the FESEM images (Figure S3, Supporting Information) reveal the structural changes from MOP crystals to discrete MOPs. Electrospray ionization mass spectroscopy (ESI-MS) clearly demonstrated the existence of discrete MOPs after the detachment process (Figure S4, Supporting Information). The ESI-MS spectra of the discrete MOPs contain only two peaks, that is, at 1607.8 and 3212.7 m/z, corresponding to $[2]^{2+}$ and $[1]^{1+}$, respectively. These distinguishable peaks confirmed that the discrete MOPs did not merge into large MOP crystals or form by-products.

To produce a MOP network film (MOP-NF), discrete MOPs were functionalized using adipoyl chloride, forming a MOP-NU via a condensation reaction between NH₂ and adipoyl chloride. A mixture of discrete MOPs and adipoyl chloride was heated in an oven at 90 °C for 2 days, yielding dark-orange MOP-NUs. The ¹H NMR spectra of the digested discrete MOPs and adipoyl chloride (Figure 2c) show the characteristic peaks induced by the benzene protons in BDC-NH₂ and the protons of aliphatic carbon in the 8.4–7.6 and 2.4–1.0 ppm ranges, respectively, confirming the occurrence of a condensation reaction. The integrated area ratio of approximately 1:4 was used to estimate the relative quantities of BDC-NH₂ and adipic acid corresponding to the two peak regions; this is consistent with the estimation that each of the six BDC-NH₂ ligands anchored each adipoyl chloride. The resultant secondary amide group donates electrons to the benzene structure, thereby dividing the three peaks, as shown by a, b, and c in Figure 2c. The protons in adipoyl chloride appear in two triplets, as shown by d and e in the figure; this is expected in an identical chemical structure. In the spectra of the MOP-NUs, the aforementioned peaks appear to be up-field shifted with respect to those of discrete MOPs and adipic acid because the amide group causes all the protons of benzene and the carbon chains to be shielded by electron-rich nitrogen and oxygen. Additionally, the absence of signals indicating by-products also confirms that the condensation reaction was successful. The full NMR spectra of digested adipoyl chloride, discrete MOP, and MOP-NU are reported in Figures S5–S7, Supporting Information. The presence of an amide group in the MOP-NUs was confirmed via Fourier transform infrared (FT-IR) spectroscopy. In the FT-IR spectrum of the MOP-NUs, the peaks at 1340 and 1480 cm⁻¹ in the blue region were significantly attenuated with respect to those of the discrete MOPs. These attenuated peaks are associated with a C–N stretching mode, indicating the restricted stretching motion of large and heavy carbon chains. Another peak appeared at 1650 cm⁻¹ and was red-shifted with respect to the peak at 1625 cm⁻¹ in the spectrum of the discrete MOPs (red region). The shift related to N–H bending vibration indicated that the primary amine was converted into a secondary amine. The peaks corresponding to the generated carbonyl groups and aliphatic carbon chains in the

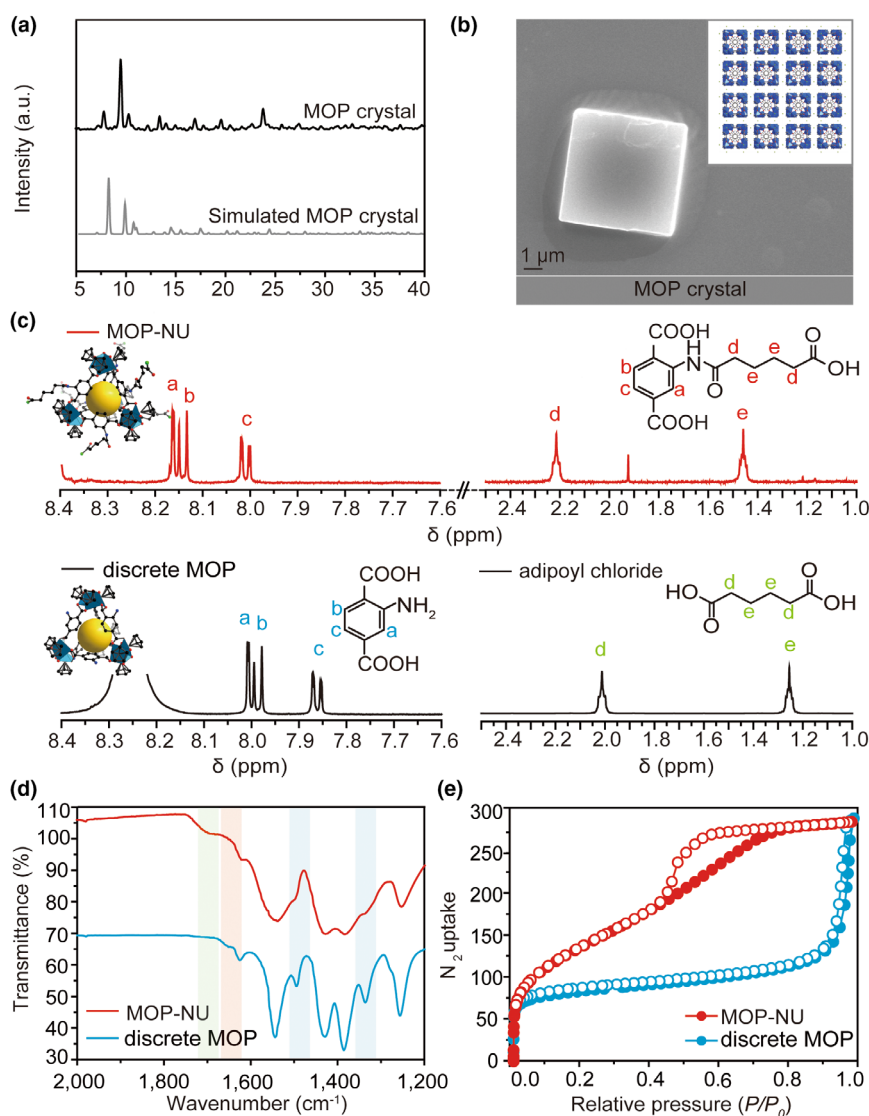


Figure 2. Characterization of the synthesized MOP crystals, discrete MOPs, and MOP-NUs. a) Powder and simulated XRD patterns of MOP crystals. b) FESEM image and illustration (inlet) of a MOP crystal. c) NMR spectra of the MOP-NUs, discrete MOPs, and adipoyl chloride. d) FT-IR spectra of the MOP-NUs and discrete MOPs. e) N₂ adsorption of the MOP-NUs and discrete MOPs.

green region appeared at 1700 cm^{-1} . The peaks corresponding to C–N, N–H, C=O, and C–C indicated that the primary amine group was converted into a corresponding amide group during the condensation reaction. The nitrogen physisorption isotherms of the MOP-NUs and the discrete MOPs displayed high amounts of adsorption at low relative pressures, indicating the presence of micropores in both materials (Figure 2e). At high relative pressures, the MOP-NUs exhibited negligible adsorption, whereas the discrete MOPs exhibited high amounts of adsorption due to pore condensation, which typically corresponds to adsorption through large pores ($>50\text{ nm}$). This difference in adsorption implies that the discrete MOPs randomly contained large inter-spaces between them, lacking sufficient force to yield a closely packed structure in a preferred direction. Interestingly, the isotherm obtained from the MOP-NUs exhibited a hysteresis and a linear uptake in the middle-relative-pressure range; this can generally be attributed to the

presence of mesopores. The carbon chains of adipic acid in the MOP-NUs generated van der Waals forces, resulting in closer proximity between the MOP-NUs with respect to that between randomly stacked MOPs.

The carbon chains introduced into the MOP-NUs increased the proximity between the MOP-NUs; based on this deduction, the formation mechanism of the MOP-NFs was investigated. First, a MOP-NU solution was prepared by considering that MOP-NUs reach saturation at a concentration of 0.8 mg mL^{-1} . The dispersion and concentration of the MOP-NUs were maintained below this threshold to ensure complete solvation (Figure S10, Supporting Information). The MOP-NU solution was subsequently spread via centrifugal forces generated during a spin-coating process, and a uniform MOP-NU layer was formed on a silicon wafer. Next, heat treatment was used to convert the MOP-NUs to MOP-NFs. To investigate the film-formation process, atomic force microscopy (AFM) was conducted to quantify the roughness and textures of the MOP-NFs prepared using different concentrations of MOP-NUs and MOPs. The five sequential steps involved in film formation using the MOP-NFs is schematically depicted in Figure 3a–e. At the lowest concentration of the MOP-NUs, the AFM images and surface topography profiles indicated that the MOP-NUs were formed as spindle-shaped structures with a height of 1.5 nm , which is consistent with the height of an individual MOP (Figure 3f and Figure S11, Supporting Information). The height of the spindle-shaped structures was approximately 1.5 nm , suggesting that the MOP-NUs attracted each other and formed one-dimensional blocks. Previous studies on tetrahedral nanoparticle packing have revealed that the lowest packing density corresponds to the formation of convex spindle-shaped structures.^[29] We hypothesized that the spindle-like structures in the MOP-NUs were formed owing to increased van der Waals

forces generated by the presence of aliphatic carbon chains. As the MOP-NU concentration increases to $1.25\text{ }\mu\text{g mL}^{-1}$ (Figure 3g), the AFM images of the MOP-NUs reveal the formation of islands. As the MOP-NU concentration increases to $5.00\text{ }\mu\text{g mL}^{-1}$, these islands merge to form a double-layered island (Figure 3h). Notably, the AFM profile of the double-layered islands shows two distinct step heights: 1.5 and 3.0 nm in the lateral and central areas, respectively. The latter height is approximately twice the height of individual MOPs, indicating that the spindle-like structures self-assembled into islands and subsequently expanded into double-layered islands without continued stacking. At a concentration of $20.00\text{ }\mu\text{g mL}^{-1}$ (Figure 3i), MOP-NFs were formed without any spindle-shaped blocks or islands. The profile of the MOP-NFs reveals low surface roughness and full coverage (Figure 3k), whereas that of the unfunctionalized MOPs shows high surface roughness with many spaces between the MOPs (Figure S12d, Supporting

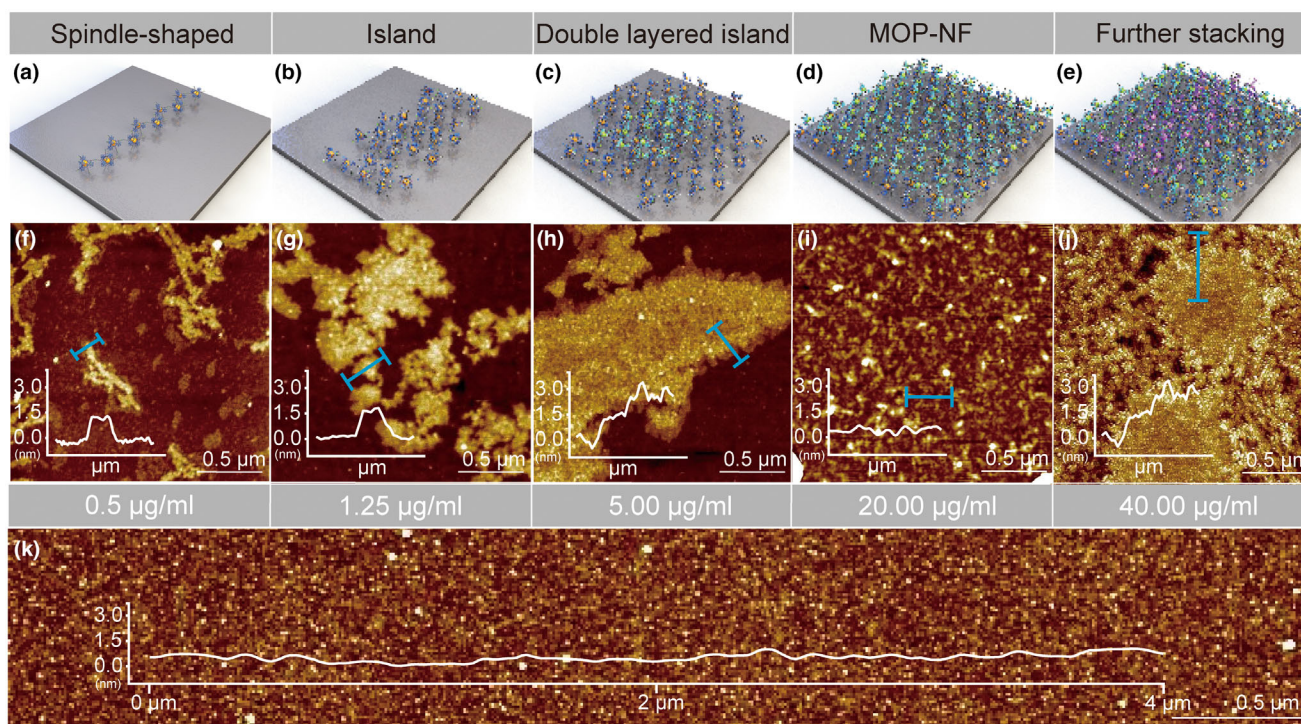


Figure 3. AFM images and profiles showing the formation of a MOP-NF. a–e) Schematic illustration of the mechanism of MOP-NFs formation following the increased concentration of MOP-NUs. f–j) AFM images and profiles corresponding to f) $0.5 \mu\text{g mL}^{-1}$, g) $1.25 \mu\text{g mL}^{-1}$, h) $5.00 \mu\text{g mL}^{-1}$, i) $20.00 \mu\text{g mL}^{-1}$, and j) $40.00 \mu\text{g mL}^{-1}$ of MOP-NFs. k) AFM image of the MOP-NFs ($20 \mu\text{g mL}^{-1}$) over a large area.

Information). When the MOP-NU concentration was above $20.00 \mu\text{g mL}^{-1}$, double-layered islands reappeared on the surface of the MOP-NFs (Figure 3j). The subsequent island formation process suggests that the thickness of the homogenous MOP-NFs can be controlled in two-layer increments of approximately 3.0 nm owing to the re-stackable nature of the films. The carbon chains of functionalized adipic acids in the MOP-NUs induce van der Waals interactions between the MOP-NUs, resulting in the formation of characteristic blocks such as spindle-shaped blocks and islands, which contribute to the formation of the homogenous microporous film. Overall, the film-formation process using MOP-NUs differs from that using MOPs only, as the latter do not form characteristic blocks and are randomly agglomerated (Figure S12, Supporting Information).

To investigate the arrangement of MOP-NUs within the MOP-NFs, grazing incidence small angle X-ray scattering (GISAXS) was conducted, as this characterization technique can reveal periodically dispersed micropores at q positions in a reciprocal space (Figure 4). The GISAXS scattering profiles of the MOP-NFs and MOPs exhibit strong reflections along the qz axis (out-of-plane axis) at $qy = 0 \text{ \AA}^{-1}$, indicating that both films were layered. Interestingly, the GISAXS scattering profile of the MOP-NFs shows patterned reflections at 29.0° and 58.1° , with the ratios at the q positions of the patterns estimated to be $1:\sqrt{3}$, that is, $0.462:0.797$ (Figure 4c,d). These angles and q -position ratios are consistent with the theoretical values, that is, 60° and $\sqrt{3}$, corresponding to a hexagonal lattice structure, indicating that MOP-NFs with hexagonal closed packing were formed.^[30,31] Additionally, the absence of peaks corresponding to the $1:\sqrt{4}$ and $1:\sqrt{7}$ ratios^[32] in the scattering pattern obtained from the MOP-NFs indicates that the films were stacked in a maximum of two

layers. The inter-distance between two MOP-NUs was calculated as 0.572 nm from the q positions of 0.788 and 1.36 nm; this inter-distance corresponds to the length of an adipoyl chloride chain. The short inter-distance between the MOP-NUs suggests that they were attracted toward each other, resulting in hexagonal closed packing with only two layers of stacking.^[33] By contrast, the GISAXS scattering profile of the MOPs showed a ring pattern that indicates that a disordered structure was present owing to the presence of randomly stacked MOPs. The distinctive differences between the GISAXS patterns indicate that the presence of one-dimensional spindle-like particles is crucial for preferentially orienting in-plane directions parallel to the substrate. Notably, the orientation difference can be attributed to the presence of functionalized adipic acids. These results suggest that the high interaction strength between the MOPs owing to the chemical modification with the adipic acids in the MOP-NUs is critical for yielding homogenous films via hermetic hexagonal packing, as inter-particle spaces are eliminated owing to dense packing of MOPs. More specifically, chemical modifications of the MOP-NUs resulted in spontaneous dense packing with hexagonal stacking in only two layers while uniformly distributed micropores occupied the interparticle spaces.

We speculated that a homogeneous film featuring uniformly spread micropores and mesopores can effectively adsorb and allow the diffusion of gas molecules. To evaluate the efficacy of the pore structures in the MOP-NFs, we initially tested the formaldehyde adsorption capacities of powder-state MOPs and MOP-NUs in a closed-loop system. Formaldehyde was chosen as an adsorbate due to its high affinity toward micropores at ambient temperatures. The closed-loop system consisted of a large gas mixing chamber connected to both a sample chamber

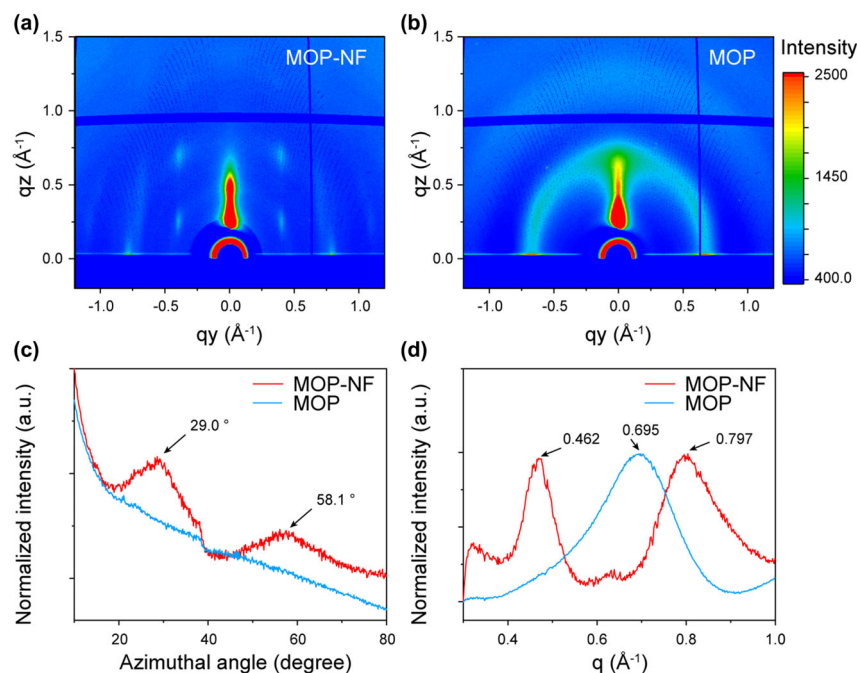


Figure 4. GISAXS scattering profiles of the MOP-NFs and MOPs. a, b) GISAXS maps of the MOP-NFs and MOPs. c, d) Intensity profiles of the MOP-NFs and MOPs.

and a gas detector (1512i photoacoustic gas monitor, LumaSense Technology).^[34,35] When the target formaldehyde concentration was reached in the gas mixing chamber using a gas control system, the formaldehyde was subsequently directed through the sample chamber. The adsorption abilities of the MOP and MOP-NU powder samples are compared in **Figure 5a**. Both the MOPs and MOP-NUs were repeatedly exposed to formaldehyde concentrations in the range of 0–45 ppm. The results indicated that the MOP-NUs adsorbed 18.8 mg g^{-1} of formaldehyde, which is more than twice that absorbed by the MOPs, that is, 7 mg g^{-1} , particularly at a formaldehyde concentration of 40 ppm. The higher amounts of adsorbed formaldehyde in the MOP-NUs than that in the MOPs implied that the mesopores formed by the close proximities between interacting MOPs provide effective transport pathways for formaldehyde.

The QCM method was used to determine the formaldehyde adsorption–desorption abilities of the MOP-NFs. The QCM method, based on the piezoelectric property of a quartz crystal, can measure extremely low mass changes owing to adsorbed gas molecules within pores during real-time monitoring.^[36] Thus, the high-quality, reliable, and accurate QCM method can be applied to comprehensively compare adsorption and diffusion efficiencies. Three different films: an adipoyl chloride (AC) film, a MOP film, and MOP-NFs were spin-coated on a QCM at 1000 g value for 20 s, followed by vacuum drying at $50 \text{ }^\circ\text{C}$ (**Figure 5b** and **Figure S14**, Supporting Information). Subsequently, the three films were placed in the sample chamber of the closed-loop system in which they were exposed to 8.5 ppm of formaldehyde molecules. The adsorption of formaldehyde onto the MOP-NFs increases the overall mass of film coated on the QCM, thereby decreasing the frequency of the QCM, which is attributable to the piezoelectric effect of the quartz crystal, as depicted in **Figure 5c**. The QCM frequency increased when the adsorbed gas was gradually desorbed upon exposure to nitrogen gas. In the QCM plot (**Figure 5d**), the

large frequency change of 45 Hz corresponding to the MOP-NFs suggests a higher formaldehyde-adsorption capacity of the MOP-NFs than those of the AC and MOP films, which exhibited frequency changes of 21 and 27 Hz, respectively. The capture and release characteristics of MOP-NU for formaldehyde are analyzed in **Figure S15**, Supporting Information, to confirm the reusability of MOP-NU as a sensor. The results demonstrate that MOP-NU can release adsorbed formaldehyde when exposed to N_2 , indicating good repeatability. By contrast, the uncoated QCM displayed only a minimal frequency variation of 4 Hz (**Figure S16**, Supporting Information).

These results imply that the MOP-NFs exhibit an effective surface interaction with formaldehyde molecules, thereby increasing mass accumulation on the film during the adsorption process. The ordered structure of the MOP-NFs facilitates the maximum utilization of the micropores and the diffusion of formaldehyde through the mesopores arising from the stationary adipic acids between the MOP-NUs, minimizing hindrance to molecular diffusion without reducing pore windows due to the presence of free adipic acids. The desorption

amount of the MOP-NFs exhibited nearly double than that of the MOPs, which indicated that the adsorbed formaldehyde escaped freely owing to the well-ordered micropores that were not blocked by other hindrances.

3. Conclusion

In this study, homogenous microporous MOP-NFs were developed by meticulously controlling the concentration of MOP-NUs and employing adipic acid functionalization. This approach facilitated the self-assembly of MOP-NUs into uniformly microporous, two-layered, hexagonally packed MOP-NFs. The MOP-NFs displayed desirable features, such as a uniform dispersion of micropores and mesopores, specific MOP orientation, and crack-free structure. Formaldehyde adsorption and desorption experiments using the QCM method revealed that the MOP-NFs possessed superior formaldehyde adsorption and desorption capacities. MOP-NFs yielded higher frequency changes of 45 Hz than 21 and 27 Hz yielded by the AC and bare MOP films, respectively. This disparity in frequency changes can be attributed to the maximum utilization of micropores in the MOP-NFs, and the mesopores between the MOP-NUs guaranteed that formaldehyde had unhindered access to the micropores. These results confirm that the functionalized discrete MOPs satisfy the criteria for producing truly homogeneous microporous films. To explore the broader applicability of MOP-NF, we propose extending its use to capture of volatile organic compounds (VOCs) such as benzene and toluene, which are commonly found in trace amounts in the environment. Given the favorable adsorption capacity of micropores for VOC sensing, we anticipate that MOP-NF, with its combination of micropores and mesopore channels, will serve as an effective material for capturing and sensing VOC compounds.

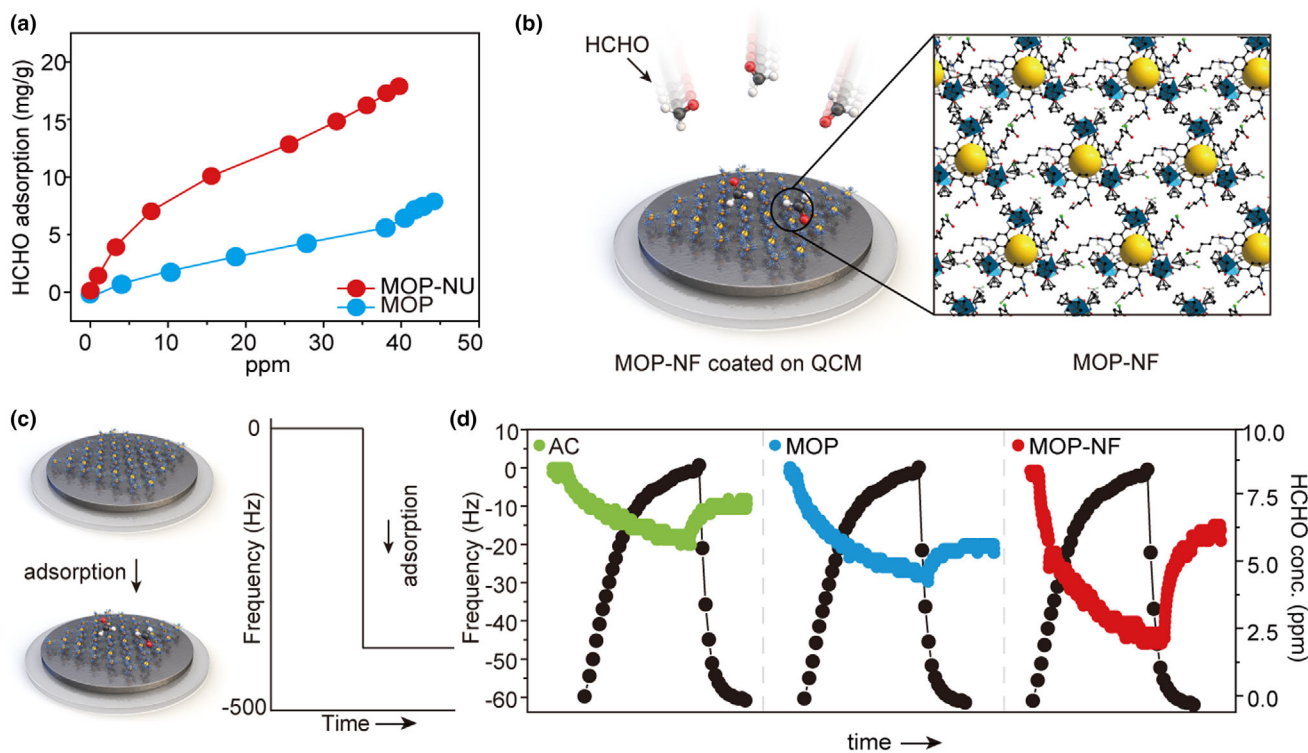


Figure 5. Formaldehyde gas adsorption and desorption experiments on the MOP-NFs using a quartz crystal microbalance (QCM). a) Formaldehyde adsorption behaviors of MOP-NU and MOP powders. b) Schematic illustration of formaldehyde gas adsorption and desorption experiments. c) Schematic illustration of the mechanism of the formaldehyde gas adsorption and desorption experiments using the QCM. d) Real-time sensor responses related to formaldehyde gas adsorption on the adipoyl chloride (AC), MOP, and MOP-NF films coated on the QCM.

4. Experimental Section

Materials: Cp_2ZrCl_2 , BDC- NH_2 , N,N-diethylformamide (DEF), acetonitrile, deionized water (DI-water), MeOH, adipoyl chloride, and triethylamine (TEA) were purchased from Sigma-Aldrich, Korea. All reagents were used as received without further purification.

Synthesis of MOPs and MOP NUs: For synthesizing MOP crystals, Cp_2ZrCl_2 (17.5 mg, 0.06 mmol), and BDC- NH_2 (5.4 mg, 0.03 mmol) were dissolved in DEF (1 mL). DI water (150 μL) was added to the mixture, followed by a reaction in an oven at 60 °C for 8 h. After the reaction, a yellow powder was obtained, which was washed three times with DEF (10 mL) in a centrifuge. For synthesizing discrete MOPs, the synthesized MOP crystals were soaked in MeOH for 3 days. A yellow MOP cage was obtained via centrifugation and dried in a freeze-dryer.

For synthesizing MOP-NUs, discrete MOPs (10.7 mg) were dissolved in a mixture of acetonitrile (1.7 mL) and DI water (1.7 mL) in a 20-mL vial. TEA (6.67 μL) was added to the solution to optimize the pH of the mixture, and the color of the solution changed to pale yellow. Adipoyl chloride was added to the solution, which changed color to transparent yellow. The preparation of the mixture was followed by a reaction in an oven at 120 °C for 2 days. After the reaction, a brown powder was obtained and washed three times with MeOH in a centrifuge.

Characterization of the MOPs and MOP-NUs: Powder XRD patterns were obtained using a Bruker D8 Advanced (TRIO/TWIN) instrument at 1600 W (40 kV and 40 mA). X-rays were scanned at 4°/min in the range of 5–20° using a Si holder. The surface morphologies and sizes of the MOPs were verified using a FESEM (JEM-7600F, JEOL). The powdered sample was dispersed in ethanol and dropped onto a holder. Additionally, ^1H NMR analysis of the digested MOPs was conducted using a Bruker Avance III HD 500 NMR spectrometer. To prepare the samples for measurement, 3 mg of dried MOPs

powder was digested and dissolved in a mixture of dimethyl sulfoxide- d_6 (700 μL) and deuterium chloride (200 μL) under sonication. An FT-IR spectrometer (Nicolet ISS0, Thermo Fisher Scientific) was used to investigate the structure of the synthesized MOP-NUs. Gas adsorption analysis was conducted using a BELSOPR-max (MicrotracBEL Corp.) gas adsorption analyzer. Samples were prepared and measured after evacuation at 120 °C for 24 h. GISAXS measurements were conducted at the 5 A beamline of the Pohang Accelerator Laboratory, Republic of Korea. The angle of the incident X-rays was maintained at 0°, and the energy of the incident photon was 11.56 keV. The patterns formed on the substrates were imaged using an AFM (Park Systems XE-100) in the noncontact mode.

Acknowledgements

This study was supported by the National Research Foundation of Korea (NRF) grant funded by the Korean Government (MSIT) (Nos. NRF-2021R1C1C2012825, 2022R1A2B5B01001826, 2022R1A5A2021216, and No. RS-2023-00218255). The authors express gratitude to Jikeun Seo for his valuable advice on the AFM experiments.

Conflict of Interest

The authors declare no competing financial interest.

Supporting Information

Supporting Information is available from the Wiley Online Library or from the author.

Keywords

formaldehyde capture, metal–organic frameworks (MOFs), metal–organic polyhedra (MOP), microporous films, self-assembly

Received: April 7, 2024

Revised: May 23, 2024

Published online: June 10, 2024

- [1] Z. Qiao, S. Zhao, M. Sheng, J. Wang, S. Wang, Z. Wang, C. Zhong, M. D. Guiver, *Nat. Mater.* **2018**, *18*, 163.
- [2] C. V. Funk, D. R. Lloyd, *J. Membr. Sci.* **2008**, *313*, 224.
- [3] A. Ambrosi, M. Pumera, *ACS Catal.* **2016**, *6*, 3985.
- [4] Y. Wang, H. Jiang, Z. Guo, H. Ma, S. Wang, H. Wang, S. Song, J. Zhang, Y. Yin, H. Wu, Z. Jiang, M. D. Guiver, *Energ. Environ. Sci.* **2023**, *16*, 53.
- [5] S. Wannapaiboon, M. Tu, K. Sumida, K. Khaletskaia, S. Furukawa, S. Kitagawa, R. A. Fischer, *J. Mater. Chem. A* **2015**, *3*, 23385.
- [6] S. Bai, X. Liu, K. Zhu, S. Wu, H. Zhou, *Nat. Energy* **2016**, *1*, 16094.
- [7] H. B. Wu, X. W. (David) Lou, *Sci. Adv.* **2017**, *3*, eaap9252.
- [8] K. M. Choi, H. M. Jeong, J. H. Park, Y.-B. Zhang, J. K. Kang, O. M. Yaghi, *ACS Nano* **2014**, *8*, 7451.
- [9] A. A. Talin, A. Centrone, A. C. Ford, M. E. Foster, V. Stavila, P. Haney, R. A. Kinney, V. Szalai, F. El Gabaly, H. P. Yoon, F. Léonard, M. D. Allen-dorf, *Science* **2013**, *343*, 66.
- [10] C. S. Lee, J. M. Lim, J. T. Park, J. H. Kim, *Chem. Eng. J.* **2021**, *406*, 126810.
- [11] H. Ji, S. Hwang, K. Kim, C. Kim, N. C. Jeong, *ACS Appl. Mater. Interfaces* **2016**, *8*, 32414.
- [12] M. C. So, S. Jin, H.-J. Son, G. P. Wiederrecht, O. K. Farha, J. T. Hupp, *J. Am. Chem. Soc.* **2013**, *135*, 15698.
- [13] D. Kim, S. Chong, C. Park, J. Ahn, J. Jang, J. Kim, I. Kim, *Adv. Mater.* **2022**, *34*, 2105869.
- [14] V. Chernikova, O. Shekhah, M. Eddaoudi, *ACS Appl. Mater. Interfaces* **2016**, *8*, 20459.
- [15] H. K. Arslan, O. Shekhah, J. Wohlgemuth, M. Franzreb, R. A. Fischer, C. Wöll, *Adv. Funct. Mater.* **2011**, *21*, 4228.
- [16] D. Jiang, A. D. Burrows, Y. Xiong, K. J. Edler, *J. Mater. Chem. A* **2013**, *1*, 5497.
- [17] K. J. Kim, J. T. Culp, P. R. Ohodnicki, P. K. Thallapally, J. Tao, *ACS Appl. Mater. Interfaces* **2021**, *13*, 35223.
- [18] C.-H. Su, C.-W. Kung, T.-H. Chang, H.-C. Lu, K.-C. Ho, Y.-C. Liao, *J. Mater. Chem. A* **2016**, *4*, 11094.
- [19] F. Al-Ghazzawi, L. Conte, C. Richardson, P. Wagner, *Angew. Chem. Int. Ed.* **2022**, *61*, 1433.
- [20] I. Stassen, M. J. Styles, G. Greci, H. V. Gorp, W. Vanderlinden, S. D. Feyter, P. Falcaro, D. D. Vos, P. M. Vereecken, R. Ameloot, *Nat. Mater.* **2016**, *15*, 304.
- [21] K. B. Lausund, M. S. Olsen, P.-A. Hansen, H. Valen, O. Nilsen, *J. Mater. Chem. A* **2020**, *8*, 2539.
- [22] H. S. Lee, S. Jee, R. Kim, H. T. Bui, B. Kim, J.-K. Kim, K. S. Park, W. Choi, W. Kim, K. M. Choi, *Energ. Environ. Sci.* **2020**, *13*, 519.
- [23] Y. J. Kim, S. Y. Ko, S. Kim, K. M. Choi, W.-H. Ryu, *Small* **2020**, *19*, 2206561.
- [24] E.-S. M. El-Sayed, D. Yuan, *Chem. Lett.* **2020**, *49*, 28.
- [25] D. Nam, J. Huh, J. Lee, J. H. Kwak, H. Y. Jeong, K. Choi, W. Choe, *Chem. Sci.* **2017**, *8*, 7765.
- [26] Z. Ji, R. Freund, C. S. Diercks, P. Hirschle, O. M. Yaghi, S. Wuttke, *Adv. Mater.* **2021**, *33*, 2103808.
- [27] G. Liu, Z. Ju, D. Yuan, M. Hong, *Inorg. Chem.* **2013**, *52*, 13815.
- [28] B. Falcon, W. Zhang, A. G. Murzin, G. Murshudov, H. J. Garringer, R. Vidal, R. A. Crowther, B. Ghetti, S. H. W. Scheres, M. Goedert, *Nature* **2018**, *561*, 137.
- [29] Y. Nagaoka, R. Tan, R. Li, H. Zhu, D. Eggert, Y. A. Wu, Y. Liu, Z. Wang, O. Chen, *Nature* **2018**, *561*, 378.
- [30] C. Hsu, K. Yue, J. Wang, X. Dong, Y. Xia, Z. Jiang, E. L. Thomas, C. Stephen, *Macromolecules* **2017**, *50*, 7282.
- [31] A. Bhattacharyya, M. K. Sanyal, U. Mogera, S. J. George, M. K. Mukhopadhyay, S. Maiti, G. U. Kulkarni, *Sci. Rep.* **2017**, *7*, 246.
- [32] H. Zhang, W. Wang, N. Hagen, I. Kuzmenko, M. Akinc, A. Travasset, S. K. Mallapragada, D. Vaknin, *Adv. Mater. Interfaces* **2016**, *3*, 1600180.
- [33] J. J. Geuchies, G. Soligno, E. Geraffy, C. P. Hendrikx, C. van Overbeek, F. Montanarella, M. R. Slot, O. V. Konovalov, A. V. Petukhov, D. Vanmaekelbergh, *Comm. Chem.* **2020**, *3*, 28.
- [34] S. Jang, S. Jee, R. Kim, J. H. Lee, H. Y. Yoo, W. Park, J. Shin, K. M. Choi, *Bull. Korean Chem. Soc.* **2021**, *42*, 315.
- [35] R. Kim, U. Ryu, S. Jee, K. Min Choi, *Appl. Surf. Sci.* **2020**, *505*, 144612.
- [36] L. Wang, *Sens. Actuator. A Phys* **2020**, *307*, 111984.